Geophysical Research Letters

RESEARCH LETTER
10.1029/2018GL079857

Magnetotail Hall Physics in the Presence of Cold Ions

L. Alm[1], M. André[1], A. Vaivads[1], Y. V. Khotyaintsev[1], R. B. Torbert[2,3], J. L Burch[3], R. E. Ergun[4], P.-A. Lindqvist[5], C. T. Russell[6], B. L. Giles[7], and B. H. Mauk[8]

[1]Swedish Institute of Space Physics, Uppsala, Sweden, [2]Space Science Center, University of New Hampshire, Durham, NH, USA, [3]Southwest Research Institute, San Antonio, TX, USA, [4]Laboratory for Atmospheric and Space Physics, University of Colorado Boulder, Boulder, CO, USA, [5]Department of Space and Plasma Physics, KTH Royal Institute of Technology, Stockholm, Sweden, [6]IGPP/EPSS, University of California, Los Angeles, CA, USA, [7]NASA Goddard Space Flight Center, Greenbelt, MD, USA, [8]Applied Physics Laboratory, Johns Hopkins University, Laurel, M, USA

Key Points:
- MMS observes mixing of cold and hot ions inside a magnetotail reconnection exhaust
- Approximately 65% of the cold ions remain magnetized even deep inside the plasma sheet
- Explaining the Hall electric field requires treating the cold and hot ions separately

Correspondence to:
L. Alm,
love.alm@irfu.se

Citation:
Alm, L., André. M., Vaivads, A., Khotyaintsev, Y. V., Torbert, R. B., & Burch, J. L. (2018). Magnetotail Hall physics in the presence of cold ions. *Geophysical Research Letters*, *45*, 10,941–10,950. https://doi.org/10.1029/2018GL079857

Received 2 AUG 2018
Accepted 17 OCT 2018
Accepted article online 22 OCT 2018
Published online 30 OCT 2018

Abstract We present the first in situ observation of cold ionospheric ions modifying the Hall physics of magnetotail reconnection. While in the tail lobe, Magnetospheric Multiscale mission observed cold (tens of eV) $\mathbf{E} \times \mathbf{B}$ drifting ions. As Magnetospheric Multiscale mission crossed the separatrix of a reconnection exhaust, both cold lobe ions and hot (keV) ions were observed. During the closest approach of the neutral sheet, the cold ions accounted for ~30% of the total ion density. Approximately 65% of the initial cold ions remained cold enough to stay magnetized. The Hall electric field was mainly supported by the $\mathbf{j} \times \mathbf{B}$ term of the generalized Ohm's law, with significant contributions from the $\nabla \cdot \mathbf{P}_e$ and $\mathbf{v}_c \times \mathbf{B}$ terms. The results show that cold ions can play an important role in modifying the Hall physics of magnetic reconnection even well inside the plasma sheet. This indicates that modeling magnetic reconnection may benefit from including multiscale Hall physics.

Plain Language Summary Cold ions have the potential of changing the fundamental physics behind magnetic reconnection. Here we present the first direct observation of this process in action in the magnetotail. Cold ions from the tail lobes were able to remain cold even deep inside the much hotter plasma sheet. Even though the cold ions only accounted for 30% of the total ions, they had a significant impact on the electric fields near the reconnection region.

1. Introduction

Magnetic reconnection is a universal process, where changes in the magnetic topology allows for mixing of plasma from different regions and conversion of magnetic energy into kinetic and thermal energy in particles. It is the driving force behind a multitude of energetic processes such as coronal mass ejections, solar flares, aurora, and geomagnetic storms. Magnetic reconnection requires that the plasma becomes demagnetized and breaks the frozen-in condition. This will typically occur when a particle species encounters structures with a characteristic length scale which is smaller than their gyro radius or inertial length. This means that the scale over which a particles species can become demagnetized depends on the particle species' mass, number density, and temperature.

In general, magnetic reconnection can be described as a two-scale process, with one length scale corresponding to the electrons and one corresponding to the heavier hydrogen ions. The ions will typically be demagnetized some distance away from the X line, whereas the electrons are only demagnetized in a narrow region surrounding the X line. This behavior leads to a differential motion between the demagnetized ions and the magnetized, $\mathbf{E} \times \mathbf{B}$ drifting, electrons. This differential motion generates the Hall current and its associated electric and magnetic fields (Nagai et al., 2001; Sonnerup, 1979). The Hall current plays an important role in that it increases the reconnection rate and introduces instabilities which may trigger reconnection onset (Birn et al., 2001; Biskamp et al., 1995, 1997; Shay et al., 2001).

Observations of dayside reconnection has found that the Hall electric field is mainly supported by the $\mathbf{j} \times \mathbf{B}$ term of the generalized Ohm's law (André et al., 2004; Khotyaintsev et al., 2006; Retinò et al., 2006). However, there are many cases where the two-scale/two-species model of magnetic reconnection is not sufficient to explain observations, one such case being when cold (thermal energy of a few tens of eV) ions (André et al., 2010;

Divin et al., 2016; Nakamura et al., 2018; Toledo-Redondo et al., 2015, 2018) or oxygen ions are present (Karimabadi et al., 2011; Markidis et al., 2011; Shay & Swisdak, 2004).

Statistical studies have shown that in the tail lobes, cold ($E < 60$ eV) ions were the dominant component in up to 70% of the observed cases (André & Cully, 2012; André et al., 2015; Engwall et al., 2009, 2008). In a low density plasma, electron capture cannot fully cancel the photoelectron current from a sunlit spacecraft, which can cause the spacecraft to charge to several tens of volts above the plasma potential (Pedersen et al., 1983). This high degree of spacecraft charging can affect the accuracy of particle and electric field measurements. Furthermore, the positive spacecraft potential will deflect ions, in particular cold ions, making it difficult to measure them directly. However, cold ions can still be observed by ion spectrometers, such as the Fast Plasma Investigation (FPI) instrument of Magnetospheric Multiscale mission (MMS), if they have a significant $\mathbf{E} \times \mathbf{B}$ drift velocity, giving them high enough energy to not be deflected by the spacecraft potential (André & Cully, 2012; Toledo-Redondo et al., 2016, 2015). Such a population of cold ions will appear as enhanced fluxes in a narrow energy range, due to their low thermal energy but with a kinetic energy which can be in the keV range. In the case of a purely $\mathbf{E} \times \mathbf{B}$ drifting population, the ions are typically confined to a narrow pitch angle range, centered at 90°. If the ions have also experienced (anti)parallel acceleration, the cold ions would still exhibit a narrow pitch angle range but would no longer be centered at 90° pitch angle. Furthermore, MMS is equipped with active spacecraft potential control, which when active keeps the spacecraft potential less than 10 V above the plasma potential, facilitating direct observations of cold ions (Torkar et al., 2016).

High geomagnetic activity is associated with increased transport of cold ions into the plasma sheet, due to an increased outflow from the ionosphere and more efficient convection transporting the cold ions to the plasma sheet, rather than allowing them to escape in the distant tail (K. Li et al., 2013). Similarly, the oxygen content of the plasma sheet has been shown to have a strong correlation with the geomagnetic activity. During storms, oxygen ions can be the dominant ion species in the plasma sheet (Kistler et al., 2005).

If cold ions enter the plasma sheet, they will typically have a gyro radius which is between that of the plasma sheet electrons and the plasma sheet ions. This introduces an intermediate length scale, where the ions can be partially magnetized. Satellite observations of dayside reconnection have shown that the presence of cold hydrogen ions tends to reduce the Hall current and thus modify the underlying microphysics of magnetic reconnection (André et al., 2010, 2016; Toledo-Redondo et al., 2015).

Heavy ions, typically oxygen, will due to their larger mass and thereby larger gyro radius introduce an additional length scale to the Hall region. Simulations have shown that compared to a hydrogen plasma, the presence of oxygen ions tends to reduce the Hall current and produce a Hall magnetic field which extends over a broader region (Markidis et al., 2011). While occurring over a different length scale, this is qualitatively similar to the effects of having a cold hydrogen ion population. In addition, the higher mass of oxygen ions will cause a reduction of the Alfvén speed, which can in turn reduce the reconnection rate (Markidis et al., 2011; Shay & Swisdak, 2004).

The effect of cold ionospheric ions on kinetic plasma physics and magnetic reconnection in the magnetotail has not been clearly established, in part due to observational constraints. Historically, two major difficulties have been producing accurate 3-D electric field measurements and particle distributions with sufficient time resolution. In this paper, we present an event from the 2017 where MMS made a partial crossing of a magnetotail reconnection exhaust, observing mixing of a cold and hot ions across the separatrix.

2. Observations

The MMS is designed to be able to resolve reconnection down to the electron scale and is with its comprehensive instrumentation well equipped for this type of study (Burch et al., 2016; Fuselier et al., 2016).

MMS measures electric and magnetic fields using the FIELDS instrument suite (Torbert et al., 2016). The FIELDS suite is in addition to the two pairs of spin-plane double probes (Lindqvist et al., 2016), also equipped with a set of axial double probes (Ergun et al., 2016). The axial double probes allow for direct measurements of the magnetotail Hall electric field, which typically is close the spin axis, $\sim Z_{GSE}$ (Geocentric solar ecliptic). The FIELDS suite measures low frequency magnetic field using two fluxgate magnetometers (FGM), one analog and one digital (Russell et al., 2016), and high frequency magnetic fields using a search-coil magnetometer (Le Contel et al., 2016).

The FPI provides distributions for low- to mid-energy (0–30 keV) electrons and ions with a time resolution of 0.03 and 0.150 s, respectively (Pollock et al., 2016). The distribution and composition of the high energy ions (20–500 keV) is provided by the Energetic Ion Spectrometer (EIS) (Mauk et al., 2016).

The event in question occurred on 6 July 2017, around 22:13 UT. MMS was at this time located near magnetic midnight, just north of the predicted plasma sheet boundary. The spacecraft separation was approximately 15 km with MMS3 and MMS4 located at the top and bottom (Z_{GSE}) of the tetrahedron.

The orientation of the plasma sheet was determined using a combination of maximum directional derivative analysis and minimum variance analysis of the magnetic field (Paschmann & Daly, 1998; Shi et al., 2005; Sonnerup & Cahill, 1967). The combined result from maximum directional derivative and minimum variance analysis of the magnetic field shows that overall, L ~ X_{GSE}, M ~ Y_{GSE}, and N ~ Z_{GSE}. The data will therefore be presented in the original GSE coordinates.

As can be seen in Figure 1a, MMS3 initially observed a strong positive B_X, B_Y of approximately −4 nT, corresponding to a guide field of ~0.15 and negligible B_Z. During this time, FPI observed a cold, low density plasma, Figures 1e and 1f. These observations are consistent with MMS being located in the northern tail lobe.

Starting at approximately 22:13:04 UT, MMS observed a gradual decrease in B_X and a positive enhancement in B_Y. During this time period, we can also begin to observe a hot ion population in the energy ranges covered by both FPI and EIS (Figures 1d and 1e), with enhanced fluxes seen up to ~80 keV. During this interval, MMS observed a gradual increase in the V_X (Figure 1b). Between 22:13:05 and 22:13:06 UT, the current exhibits oscillations close to the lower-hybrid frequency (~10 Hz). After 22:13:06 UT, we observe a stable J_Y current sheet. This indicates that MMS had crossed the separatrix between the northern tail lobe and the plasma sheet and was gradually moving toward the neutral sheet.

At approximately 22:13:07.5 UT, we observed a minimum in B_X, 7.2 nT, after which B_X, V_X, and J_Y gradually returned to lobe values, indicating that MMS was moving away from the neutral sheet. Starting at 22:13:14 UT, neither FPI nor EIS detects any high energy ions, and B_X is in excess of 20 nT, suggesting that MMS has crossed the separatrix and reentered the northern tail lobe. During the outbound crossing the current is dominated by oscillations, with an amplitude of ~ 20 nA/m^2, with a frequency close to the lower-hybrid frequency (~10 Hz).

We performed a Walén test to investigate if the ion jet could be associated with reconnection. The event does not have a well-defined deHoffman-Teller frame, exhibiting large variations between different spacecraft. The frame velocity is between ~1,800 and ~2,600 km/s, which is unrealistically large compared to the 200–400 km/s given by timing analysis. Therefore, we performed the Walen test in the spacecraft frame, which can be expressed as

$$\Delta \mathbf{v}_i = \pm \Delta \mathbf{v}_A, \tag{1}$$

where $\mathbf{v}_i$ is the ion velocity, and $\mathbf{v}_A$ is the Alfvén velocity; the Δ denotes the change relative a reference value, in our case the lobe values (Paschmann & Daly, 2008; Phan et al., 2004). The Alfvén velocity with corrections for pressure anisotropy is expressed as

$$v_A = \mathbf{B}\left[(1-\alpha)/\mu_0\rho\right]^{0.5}, \tag{2}$$

where $\alpha = \left(p_{||} - p_{\perp}/\mu_0/B^2\right)$ is the pressure anisotropy, μ_0 is the vacuum permeability, and ρ the density (Paschmann & Daly, 2008). As can be seen in Figure 1g, ion acceleration is strongly correlated with the change in Alfvén velocity. Across MMS, the increase in ion velocity is between 71% and 92% of the change in Alfvén velocity, consistent with by magnetotail reconnection (Eriksson et al., 2004; Øieroset et al., 2000). Note that FPI cannot detect the ions with the highest energies and that the ion moments may underestimate the ion bulk velocity. The positive V_X jet would therefore suggest that MMS was located Earthward of the X line. The large V_Y jet observed during the outbound leg is predominately perpendicular to the magnetic field, indicating cross tail motion of the plasma sheet.

The motion of the plasma sheet was estimated using the spatiotemporal difference method, relying on the B_X and B_Y components of the magnetic field (Denton et al., 2016; Shi et al., 2005). Using the results from the motion analysis, we used the Harris sheet approximation to fit B_X as a function of the position in Z_{GSE} (Harris, 1962). As can be seen in Figure 1h, the Harris sheet model provides a good fit to our observations, especially during the inbound crossing. The outbound crossing exhibits a more complicated motion, which could explain some of the deviations from out model. There is also a small J_Y current sheet and wave activity near

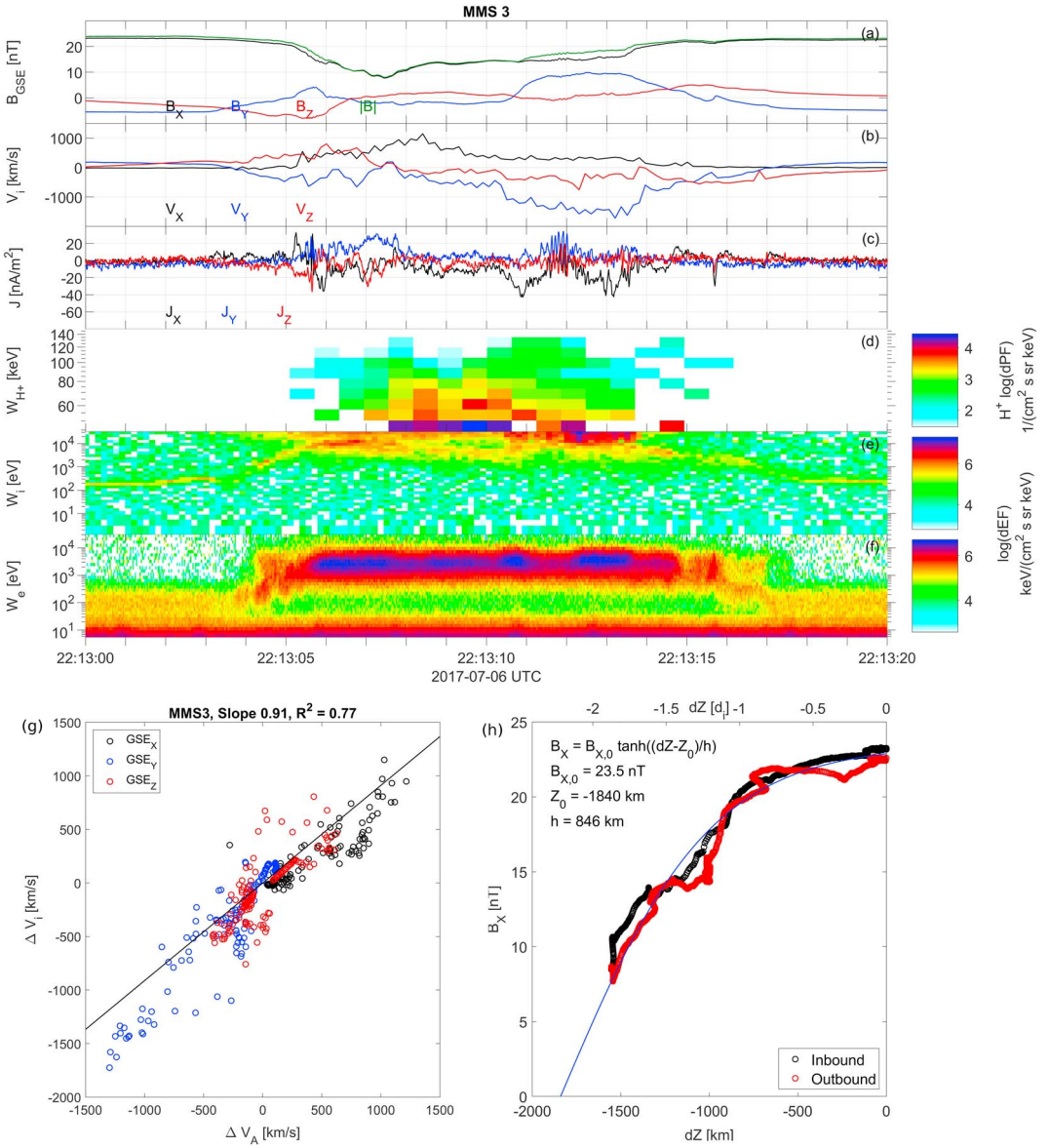

Figure 1. Overview of event as observed by MMS3. (a) Magnetic field. (b) Ion bulk velocity. (c) Currents calculated using the curlometer method. (d) Proton energy spectrogram (Energetic Ion Spectrometer). (e) Ion energy spectrogram (FPI). (f) Electron energy spectrogram (FPI). (g) Walén test calculated using velocities from FPI. (h) B_X fit to a Harris sheet. FPI = Fast Plasma Investigation; MMS = Magnetospheric Multiscale mission.

the separatrix which complicates the analysis. This allows us to estimate the characteristic length scale of the Harris sheet to ~850 km and extrapolate that the closest distance to the neutral sheet was ~300 km or ~0.4 lobe ion skin depths (d_i).

Given the motion of magnetic structure, reexamining the magnetic field shows that the large scale bipolar B_Z signature, observed between 22:13:03 and 22:13:18 UT, is not associated with crossing an X line. Given the initial direction of the ion jet and motion of MMS, such a signature should have the opposite polarity. The B_Z signature is among other things consistent with either a small magnetic island embedded in the exhaust, a plasma sheet bulge propagating Earthward or a corrugated plasma sheet. The enhanced B_Y observed both during the inbound and outbound crossings of the separatrix is consistent with the expected orientation of the Hall magnetic field northward and Earthward of an X line.

Figure 2 shows the ion energy and pitch angle spectrograms from FPI between 22:13:02 and 22:13:17 UT, during which MMS observed the partial plasma sheet crossing. As can be seen in Figure 2b, before and after the

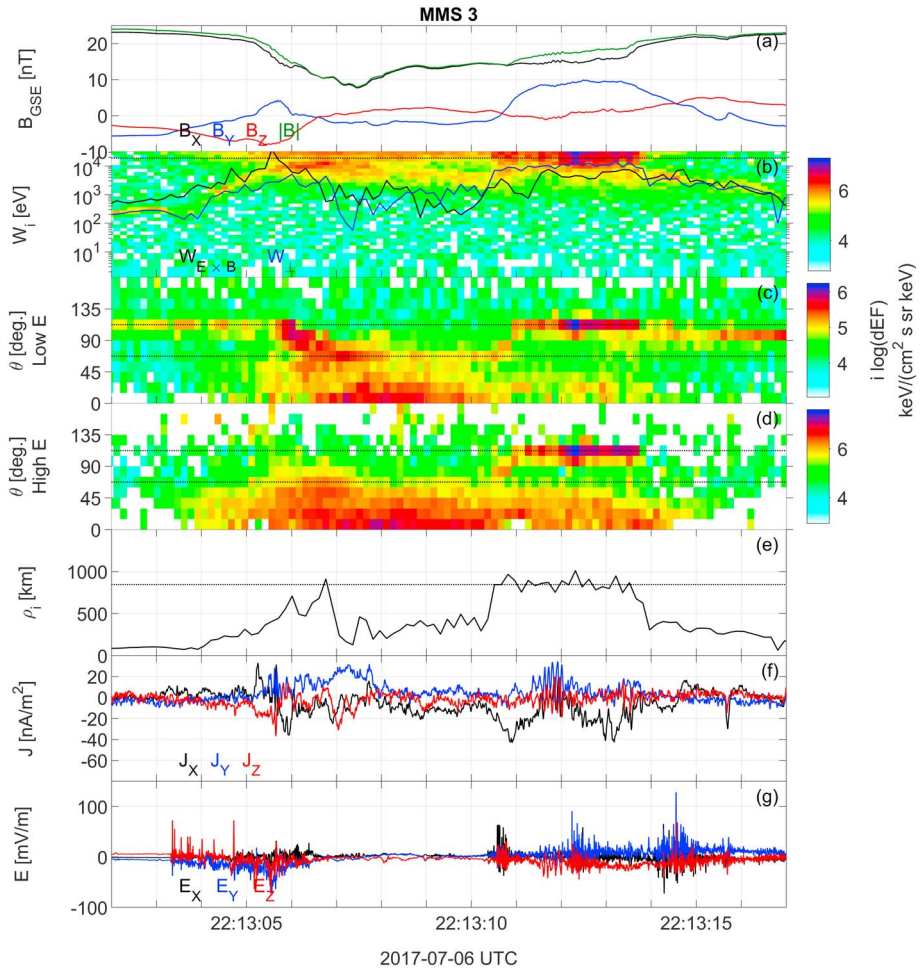

Figure 2. Electron and ion spectrograms from MMS3. (a) Magnetic field. (b) Ion energy spectrogram (FPI). The solid black line shows the **E** × **B** velocity estimated from FIELDS data, the solid blue line shows the energy corresponding to the perpendicular component of the ion bulk velocity, and the black-dashed line indicates the cutoff energy of separating the cold and hot ion populations. (c) Ion pitch angle spectrogram for E < 18,800 eV (FPI). The dashed lines indicates the pitch angle range of the cold ions. (d) Ion pitch angle spectrogram for E > 18,800 eV (FPI). The dashed lines indicates the pitch angle range of the cold ions. (e) Gyro radius of a proton. Calculated from the ion bulk velocity. (f) Currents calculated using the curlometer method (FGM). (g) Electric fields Electric Double Probes. FPI = Fast Plasma Investigation; MMS = Magnetospheric Multiscale mission.

plasma sheet crossing, MMS observed a population of cold but accelerated ions, that is, they have low thermal velocity (spread in energy) but high bulk velocity (total energy). The enhanced energy of these cold ions is the result of a significant **E** × **B** drift velocity, evident from enhanced fluxes around the energy corresponding to the local **E** × **B** velocity. This is further supported by the observation that the cold ions were focused into a narrow region around 90° pitch angle (Figure 2c). These cold **E** × **B** drifting ions were a persistent feature and could be observed during the entire 25-min period which MMS spends in the lobe prior to and after this event (not shown).

Starting at approximately 22:13:04 UT, as MMS started moving into the plasma sheet, the cold ions were gradually accelerated to energies >1 keV but exhibiting little heating. At 22:13:05 UT, MMS began to observe a hot ion population in the top energy channels of FPI. At 22:13:06 UT, the cold ions have through a combination of acceleration and, to a lesser degree heating, reached an energy of ~15 keV. However, the cold and hot ions are still separated by a slot region located at ~19 keV. This higher energy cutoff of the cold ions can also be seen clearly between 22:13:07.8 and 22:13:10.4 UT. Both the cold and hot ions are enhanced for pitch angles <135°, but the hotter ions dominate for pitch angles <60°.

Starting at ~22:13:10 UT, MMS made its second, outbound pass of the separatrix. It is here MMS observed the strongest DC E_Z, corresponding to the Hall electric field. Here the cold ion population has been accelerated, but not heated significantly, to high enough energies that the two ion populations cannot be easily separated in the energy spectrogram. However, as we can see in Figures 2c and 2d, the cold ions stand out as a clear enhancement at ~105° pitch angle, whereas the hot ions are for the most part confined to pitch angles <60°.

Figure 2e shows the hydrogen gyro radius, calculated from the average perpendicular ion energy measured by FPI. The dashed line indicates the length scale of the Harris current sheet, determined from Figure 1h. Since FPI moments are used, the high energy ions which are observed by EIS are not accounted for. Ions with a gyro radius larger that the length scale of the current sheet will not remain fully magnetized. The cold ions observed in the lobes have a gyro radius which is much smaller than the length scale of the Harris sheet and can, if they are not heated significantly, remain magnetized inside the plasma sheet. The solid blue line in Figure 2b shows the perpendicular energy corresponding to this gyro radius. As can be seen in Figures 1c and 1d, the hot ion population extends to energies of 80 keV, these ions are likely to have a large enough gyro radius to be partially of fully demagnetized.

In order to study the influence of the two ion populations on the Hall electric field, we formulate a generalized Ohm's law with terms for electrons, cold ions, and hot ions. EIS and HPCA (Hot Plasma Composition Analyzer) indicate that heavier ions are present but that they only account for <1% of the total number density. We will therefore assume that we are dealing with a pure hydrogen plasma. For this case, the observed electric field **E** can be expressed as

$$\mathbf{E} = \frac{1}{en}\mathbf{j}\times\mathbf{B} - \frac{n_c}{n}\mathbf{v_c}\times\mathbf{B} - \frac{n_h}{n}\mathbf{v_h}\times\mathbf{B} - \frac{1}{en}\nabla\cdot\mathbf{P_e}, \tag{3}$$

where e is the elemental charge, n is the plasma density, **j** is the current calculated using the curlometer method (Paschmann & Daly, 2008), **B** is the magnetic field, n_c and n_h are the densities of the cold and hot ions, respectively, $\mathbf{v_c}$ and $\mathbf{v_h}$ are the bulk velocity of the cold and hot ions,respectively, and $\nabla\cdot\mathbf{P_e}$ is the divergence of the electron pressure tensor, which is calculated across the MMS tetrahedron. The terms corresponding to effects of electron inertia are omitted since they can be safely ignored over scales much larger than the electron inertial length (André et al., 2016; Toledo-Redondo et al., 2015).

The density and bulk velocity of the cold ions are calculated by restricting the moment integrations to energies lower than 18.8 keV, the cutoff energy seen in Figure 2b, and with a pitch angle range of 90 ± 22.5 °, corresponding to the range seen in Figures 2c and 2d. Since FPI can only capture the low energy tail of the hot plasma sheet ions, FPI cannot produce accurate moments for the hot ions. Fortunately, FPI can sample the bulk of the electrons, and by assuming quasi-neutrality, $n_e = n_i = n_c + n_h$, we can estimate the hot ion density. In theory, the bulk velocity of the hot ions could be estimated from the curlometer current since

$$\mathbf{j} = e(n_c\mathbf{v_c} + n_h\mathbf{v_h} - n_e\mathbf{v_e}). \tag{4}$$

However, such an estimate would contain the compound errors of curlometer current as well as the electron and cold ion moments, greatly reducing its accuracy. Instead, we will for now assume that $\mathbf{v_h}\times\mathbf{B} = 0$, which, as discussed previously, is expected based on the gyro radius of the hot ions and the length scale of the Harris current sheet. The hot ions are still accounted for, if indirectly, by the curlometer current and in the fact that $n_h \neq 0 \rightarrow n_c/n < 1$, which reduces the contribution from the $(n_c/n)\mathbf{v_c}\times\mathbf{B}$ term.

Figure 3 compares the electric field, particle motion, and their relative contributions from the different terms of the generalized Ohm's law (equation (3)). The smoother appearance of the ions is partially due to the lower sample rate than the electrons, 0.03 versus 0.150 s, but can mainly be attributed to their higher mass preventing them from responding to rapidly fluctuating electric fields or small scale structures.

As can be seen in Figures 3b–3e, for the most part, the observed normal electric field, $-\mathbf{v_e}\times\mathbf{B}$, and $-\mathbf{v_c}\times\mathbf{B}$ are in good agreement, indicating frozen-in behavior from electrons and cold ions. One notable exception is observed between 22:13:10.5 and 22:13:12 UT where both the cold ions and the electrons exhibit a deviation from the observed electric field. If this was only observed in the ions, one could suspect that the issue in how the cold ion moments were calculated. Since that is not the case, it may indicate a degree of nonideal motion in both the electrons and cold ions.

Since both the curlometer current and the divergence of the electron pressure are calculated across the MMS tetrahedron, Figures 3f–3h will use the barycentric average of all quantities. Figure 3f shows the relative density contribution from cold and hot ions. Initially, all of the ions are cold, and the density is approximately

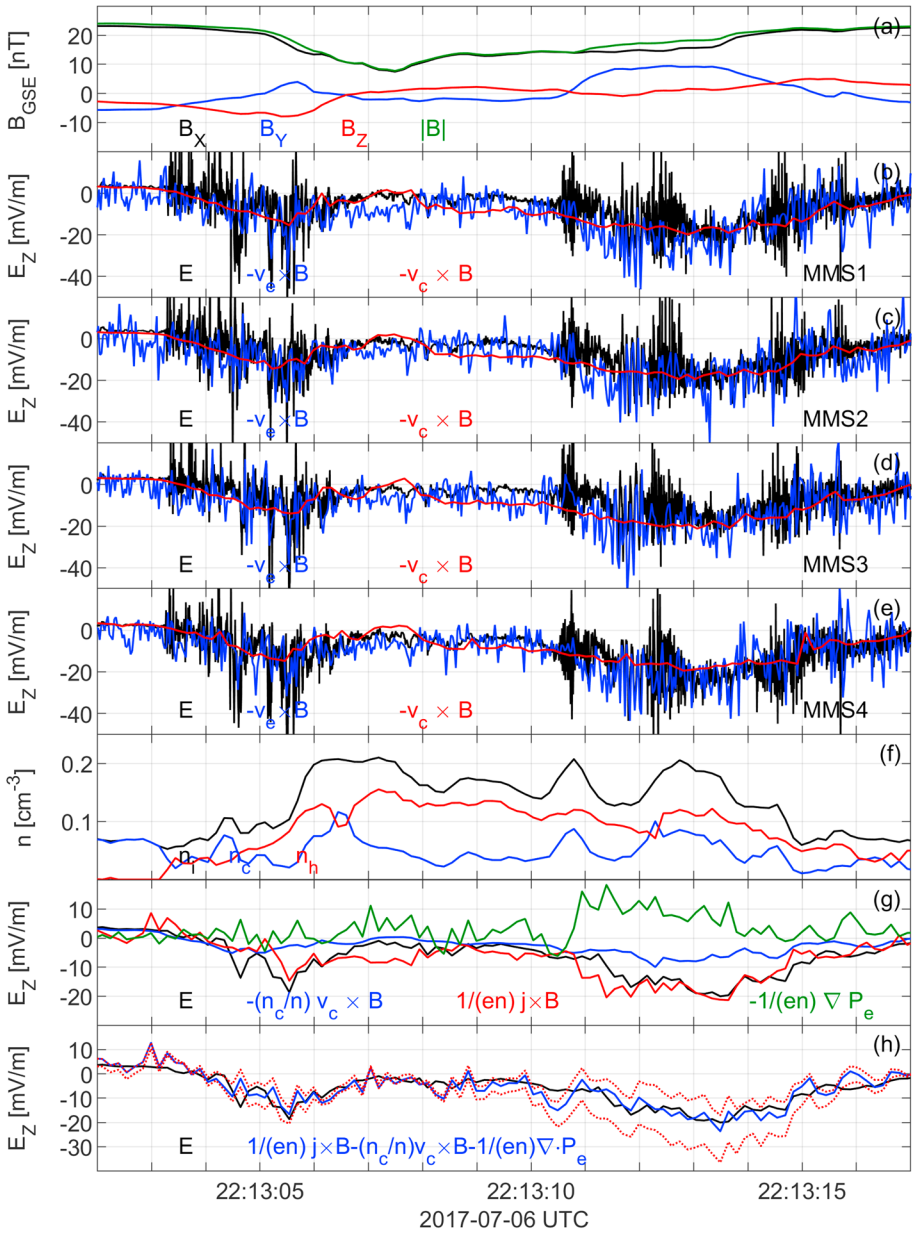

Figure 3. Comparison of observed electric field, particle bulk motion, and contributions to Ohm's law. (a) Magnetic field observed by MMS3. (b–e) Comparison of E_Z, $[-\mathbf{v_e} \times \mathbf{B}]_Z$ and $[-\mathbf{v_c} \times \mathbf{B}]_Z$ from MMS1 to MMS4. (f) Ion density: total (black), cold (blue), and hot (red). (g) Comparison of the terms of Ohm's law. (h) Comparison of observed electric field and sum of the right hand side of Ohm's law. The red-dashed lines indicate the outcome if one assumes all ions are cold/magnetized or that all ions are hot/demagnetized. MMS = Magnetospheric Multiscale mission.

0.07/cm^3. This number is agreement with the density derived from the observed electron plasma frequency (not shown). The cold ions are observed throughout the partial plasma sheet crossing though their density decrease as we move deeper into the plasma sheet. On average, they account for ~30% of the total ion density.

In Figure 3g, we compare the observed E_Z Hall electric field with the various terms of the right-hand side of equation (3). In this panel, the electric field and electron moments have been down-sampled to the same time resolution as the ion moments. The largest contributor to the Hall electric field is the $\mathbf{j} \times \mathbf{B}$ term, this is similar to previous results from dayside reconnection (André & Cully, 2012; Toledo-Redondo et al., 2016, 2015). The fact that we have a strong $\mathbf{j} \times \mathbf{B}$ term despite that both the electrons and cold ions are magnetized shows that the hot ions are not.

The electron pressure term is as expected pointing away from the X line. It is on average ~40% of the $\mathbf{j} \times \mathbf{B}$ term, which is considerably larger than expected from similar studies at the dayside magnetopause (André et al., 2016; Khotyaintsev et al., 2006; Toledo-Redondo et al., 2015), as well as simulations (Aunai et al., 2013). The large electron pressure term does not appear to be an artifact introduced by noise when calculating the pressure gradient. Inspecting the data shows that there is a clear and consistent difference in the diagonal terms of the electron pressure tensor, but not in the off-diagonal terms, between the MMS3 which is at the top (Z_{GSE}) of the tetrahedron and MMS4 which is at the bottom. The large electron pressure term may indicate that the electrons are not fully frozen-in, as $\mathbf{E} + \mathbf{v_e} \times \mathbf{B} \neq 0$. Electron demagnetization has not only been observed inside the electron diffusion region (EDR) but has also been predicted and observed and along separatrices in close proximity to the X line, sometimes referred to as the outer EDR (Hwang et al., 2017; Scudder et al., 2008).

The magnitude of the $(n_c/n)\mathbf{v_c}\times\mathbf{B}$ term is for the most part <5 mV/m. During the outbound separatrix crossing, where the Hall electric field is the strongest, $(n_c/n)\mathbf{v_c} \times \mathbf{B}$ term is between 5 and 10 mV/m compared to the ~20 mV/m contribution from the $\mathbf{j} \times \mathbf{B}$ term. This makes it the weakest of the three terms but still finite and nonnegligible.

The blue line in Figure 3h shows the sum of all terms of the right-hand side of Ohm's law, which for the most part does an excellent job of estimating the observed electric field. There is a slight tendency for underestimating the electric field, this is especially clear between 22:13:04–22:13:06 and 22:13:11–22.13:17 UT. This is likely to be the consequence of underestimating the cold ion density rather than errors in the velocity. Going back to Figure 2, we can see that after 22:13:15 UT, we do not observe any hot plasma; thus, we would expect that $n_c = n_i$. However, as can be seen in Figure 3f, this is not the case. The two red-dashed lines in Figure 3h indicate the two extreme cases, assuming that all ions are cold and magnetized or assuming all ions are hot and demagnetized. This illustrates the large range of solutions that are possible depending on the treatment of the ions. This shows that the good agreement between the observed normal electric field and our modified generalized Ohm's law is not merely coincidental nor the result of the ions having a negligible influence.

3. Conclusions and Summary

In this event the cold ions account for ~30% of the total plasma sheet ion density. Approximately ~65% of the initially cold ion population remained cold even during the closest approach to the neutral sheet. The cold, magnetized ions were observed ~1,000 km (1.2 d_i) into the plasma sheet. This shows that cold ions can penetrate a significant distance into the plasma sheet. This is the first study showing that cold, ionospheric ions are an important factor in governing the Hall physics in the magnetotail. This is similar to results from the dayside magnetopause, where cold ions has been observed deep inside the reconnection exhaust (W. Y. Li et al., 2017).

In order to accurately describe the observed Hall electric field, we have to invoke three terms of our generalized Ohm's law, $\mathbf{j} \times \mathbf{B}$, $(n_c/n)\mathbf{v_c} \times \mathbf{B}$, and $\nabla \cdot \mathbf{P_e}$. The term corresponding to the hot ions, $(n_h/n)\mathbf{v_h} \times \mathbf{B}$, was not required to explain the observed Hall field. This indicates that despite being the major ion component, the hot ions did not contribute significantly to the Hall field, indicating that they were fully demagnetized. Instead, the hot ions manifest as part of the Hall current, which would be zero if the hot ions were also fully magnetized.

In conclusion, cold ions can have a significant influence the Hall physics even when they are a minor species. These cold ions succeed in penetrating a significant distance into the plasma sheet without being heated to the degree that they become demagnetized. This implies that realistic modeling of magnetic reconnection must take cold ions into account and consider the multiscale view of Hall physics.

Acknowledgments
This paper was made possible by the hard work of all members of the MMS Team. All data used in this paper are publicly available at MMS Science Data Center (https://lasp.colorado.edu/mms/sdc/public/). We acknowledge support by the Swedish National Space Agency contracts SNSB 176/15 and 158/16.

References

André, M., & Cully, C. M. (2012). Low-energy ions: A previously hidden solar system particle population. *Geophysical Research Letters*, *39*, L03101. https://doi.org/10.1029/2011GL050242

André, M., Li, K., & Eriksson, A. I. (2015). Outflow of low-energy ions and the solar cycle. *Journal of Geophysical Research: Space Physics*, *120*, 1072–1085. https://doi.org/10.1002/2014JA020714

André, M., Li, W., Toledo-Redondo, S., Khotyaintsev, Y. V., Vaivads, A., Graham, D. B., et al. (2016). Magnetic reconnection and modification of the Hall physics due to cold ions at the magnetopause. *Geophysical Research Letters*, *43*, 6705–6712. https://doi.org/10.1002/2016GL069665

André, M., Vaivads, A., Buchert, S. C., Fazakerley, A., & Lahiff, A. (2004). Thin electron-scale layers at the magnetopause. *Geophysical research letters*, *31*, L03803. https://doi.org/10.1029/2003GL018137

André, M., Vaivads, A., Khotyaintsev, Y. V., Laitinen, T., Nilsson, H., Stenberg, G., et al. (2010). Magnetic reconnection and cold plasma at the magnetopause. *Geophysical Research Letters*, *37*, L22108. https://doi.org/10.1029/2010GL044611

Aunai, N., Hesse, M., Zenitani, S., Kuznetsova, M., Black, C., Evans, R., & Smets, R. (2013). Comparison between hybrid and fully kinetic models of asymmetric magnetic reconnection: Coplanar and guide field configurations. *Physics of Plasmas*, *20*(2), 022902. https://doi.org/10.1063/1.4792250

Birn, J., Drake, J., Shay, M., Rogers, B., Denton, R., Hesse, M., et al. (2001). Geospace environmental modeling (GEM) magnetic reconnection challenge. *Journal of Geophysical Research*, *106*(A3), 3715–3719.

Biskamp, D., Schwarz, E., & Drake, J. (1995). Ion-controlled collisionless magnetic reconnection. *Physical Review Letters*, *75*(21), 3850.

Biskamp, D., Schwarz, E., & Drake, J. F. (1997). Two-fluid theory of collisionless magnetic reconnection. *Physics of Plasmas*, *4*(4), 1002–1009. https://doi.org/10.1063/1.872211

Burch, J., Moore, T., Torbert, R., & Giles, B. (2016). Magnetospheric Multiscale overview and science objectives. *Space Science Reviews*, *199*(1–4), 5–21.

Denton, R. E., Sonnerup, B. U., Hasegawa, H., Phan, T. D., Russell, C. T., Strangeway, R. J., et al. (2016). Motion of the MMS spacecraft relative to the magnetic reconnection structure observed on 16 october 2015 at 1307 UT. *Geophysical Research Letters*, *43*, 5589–5596. https://doi.org/10.1002/2016GL069214

Divin, A., Khotyaintsev, Y. V., Vaivads, A., André, M., Toledo-Redondo, S., Markidis, S., & Lapenta, G. (2016). Three-scale structure of diffusion region in the presence of cold ions. *Journal of Geophysical Research: Space Physics*, *121*, 12,001–12,013. https://doi.org/10.1002/2016JA023606

Engwall, E., Eriksson, A. I., Cully, C. M., AndrA, M., Torbert, R., & Vaith, H. (2008). Earth's ionospheric outflow dominated by hidden cold plasma. *Nature Geoscience*, *2*(4), 321–324.

Engwall, E., Eriksson, A. I., Cully, C. M., André, M., Puhl-Quinn, P. A., Vaith, H., & Torbert, R. (2009). Survey of cold ionospheric outflows in the magnetotail. *Annales Geophysicae*, *27*(8), 3185–3201. https://doi.org/10.5194/angeo-27-3185-2009

Ergun, R. E., Tucker, S., Westfall, J., Goodrich, K. A., Malaspina, D. M., Summers, D., et al. (2016). The axial double probe and fields signal processing for the MMS mission. *Space Science Reviews*, *199*(1), 167–188. https://doi.org/10.1007/s11214-014-0115-x

Eriksson, S., Øieroset, M., Baker, D., Mouikis, C., Vaivads, A., Dunlop, M., et al. (2004). Walén and slow-mode shock analyses in the near-Earth magnetotail in connection with a substorm onset on 27 August 2001. *Journal of Geophysical Research*, *109*, A10212. https://doi.org/10.1029/2004JA010534

Fuselier, S. A., Lewis, W. S., Schiff, C., Ergun, R., Burch, J. L., Petrinec, S. M., & Trattner, K. J. (2016). Magnetospheric Multiscale science mission profile and operations. *Space Science Reviews*, *199*(1–4), 77–103.

Harris, E. G. (1962). On a plasma sheath separating regions of oppositely directed magnetic field. *Il Nuovo Cimento (1955-1965)*, *23*(1), 115–121.

Hwang, K.-J., Sibeck, D., Choi, E., Chen, L.-J., Ergun, R., Khotyaintsev, Y., et al. (2017). Magnetospheric Multiscale mission observations of the outer electron diffusion region. *Geophysical Research Letters*, *44*, 2049–2059. https://doi.org/10.1002/2017GL072830

Karimabadi, H., Roytershteyn, V., Mouikis, C., Kistler, L., & Daughton, W. (2011). Flushing effect in reconnection: Effects of minority species of oxygen ions. *Planetary and Space Science*, *59*(7), 526–536.

Khotyaintsev, Y. V., Vaivads, A., Retinò, A., André, M., Owen, C., & Nilsson, H. (2006). Formation of inner structure of a reconnection separatrix region. *Physical Review Letters*, *97*(20), 205003.

Kistler, L. M., Mouikis, C., Möbius, E., Klecker, B., Sauvaud, J. A., RÃme, H., et al. (2005). Contribution of nonadiabatic ions to the cross-tail current in an O^+ dominated thin current sheet. *Journal of Geophysical Research*, *110*, A06213. https://doi.org/10.1029/2004JA010653

Le Contel, O., Leroy, P., Roux, A., Coillot, C., Alison, D., Bouabdellah, A., et al. (2016). The search-coil magnetometer for MMS. *Space Science Reviews*, *199*(1), 257–282. https://doi.org/10.1007/s11214-014-0096-9

Li, W. Y., André, M., Khotyaintsev, Y. V., Vaivads, A., Fuselier, S. A., Graham, D. B., et al. (2017). Cold ionospheric ions in the magnetic reconnection outflow region. *Journal of Geophysical Research: Space Physics*, *122*, 10,194–10,202. https://doi.org/10.1002/2017JA024287

Li, K., Haaland, S., Eriksson, A., André, M., Engwall, E., Wei, Y., et al. (2013). Transport of cold ions from the polar ionosphere to the plasma sheet. *Journal of Geophysical Research: Space Physics*, *118*, 5467–5477. https://doi.org/10.1002/jgra.50518

Lindqvist, P.-A., Olsson, G., Torbert, R. B., King, B., Granoff, M., Rau, D., et al. (2016). The spin-plane double probe electric field instrument for MMS. *Space Science Reviews*, *199*(1), 137–165. https://doi.org/10.1007/s11214-014-0116-9

Markidis, S., Lapenta, G., Bettarini, L., Goldman, M., Newman, D., & Andersson, L. (2011). Kinetic simulations of magnetic reconnection in presence of a background O^+ population. *Journal of Geophysical Research*, *116*, A00K16. https://doi.org/10.1029/2011JA016429

Mauk, B., Blake, J., Baker, D., Clemmons, J., Reeves, G., Spence, H. E., et al. (2016). The energetic particle detector (EPD) investigation and the energetic ion spectrometer (EIS) for the Magnetospheric Multiscale (MMS) mission. *Space Science Reviews*, *199*(1–4), 471–514.

Nagai, T., Shinohara, I., Fujimoto, M., Hoshino, M., Saito, Y., Machida, S., & Mukai, T. (2001). Geotail observations of the Hall current system: Evidence of magnetic reconnection in the magnetotail. *Journal of Geophysical Research*, *106*(A11), 25,929–25,949.

Nakamura, R., Varsani, A., Genestreti, K. J., Le Contel, O., Nakamura, T., Baumjohann, W., et al. (2018). Multiscale currents observed by MMS in the flow braking region. *Journal of Geophysical Research: Space Physics*, *123*, 1260–1278. https://doi.org/10.1002/2017JA024686

Øieroset, M., Phan, T. D., Lin, R. P., & Sonnerup, B. U. (2000). Walén and variance analyses of high-speed flows observed by wind in the midtail plasma sheet: Evidence for reconnection. *Journal of Geophysical Research*, *105*(A11), 25,247–25,263.

Paschmann, G., & Daly, P. W. (1998). *Analysis methods for multi-spacecraft data* (1.1 ed.). Noordwijk, Netherlands: ESA Publications Division.

Paschmann, G., & Daly, P. W. (2008). *Multi-spacecraft analysis methods revisited*. Noordwijk, Netherlands: ESA Publications Division.

Pedersen, A., Chapell, C., Knott, K., & Olsen, R. (1983). Methods for keeping a conductive spacecraft near the plasma potential. In *Proceedings of the 17th ESLAB Symposium Spacecraft Plasma Interactions and Their Influence on Field and Particle Measurements, ESA SP-198, Citeseer* (pp. 185–190).

Phan, T. D., Dunlop, M. W., Paschmann, G., Klecker, B., Bosqued, J. M., Rème, H., et al. (2004). Cluster observations of continuous reconnection at the magnetopause under steady interplanetary magnetic field conditions. *Annales Geophysicae*, *22*(7), 2355–2367.

Pollock, C., Moore, T., Jacques, A., Burch, J., Gliese, U., Saito, Y., et al. (2016). Fast plasma investigation for Magnetospheric Multiscale. *Space Science Reviews*, *199*(1), 331–406. https://doi.org/10.1007/s11214-016-0245-4

Retinò, A., Vaivads, A., André, M., Sahraoui, F., Khotyaintsev, Y., Pickett, J., et al. (2006). Structure of the separatrix region close to a magnetic reconnection X-line: Cluster observations. *Geophysical Research Letters*, *33*, L06101. https://doi.org/10.1029/2005GL024650

Russell, C. T., Anderson, B. J., Baumjohann, W., Bromund, K. R., Dearborn, D., Fischer, D., et al. (2016). The Magnetospheric Multiscale magnetometers. *Space Science Reviews*, *199*(1), 189–256. https://doi.org/10.1007/s11214-014-0057-3

Scudder, J., Holdaway, R., Glassberg, R., & Rodriguez, S. (2008). Electron diffusion region and thermal demagnetization. *Journal of Geophysical Research*, *113*, A10208. https://doi.org/10.1029/2008JA013361

Shay, M. A., Drake, J. F., Rogers, B. N., & Denton, R. E. (2001). Alfvénic collisionless magnetic reconnection and the Hall term. *Journal of Geophysical Research*, *106*(A3), 3759.

Shay, M. A., & Swisdak, M. (2004). Three-species collisionless reconnection: Effect of O^+ on magnetotail reconnection. *Physical Review Letters*, *93*(175), 001. https://doi.org/10.1103/PhysRevLett.93.175001

Shi, Q. Q., Shen, C., Pu, Z. Y., Dunlop, M. W., Zong, Q.-G., Zhang, H., et al. (2005). Dimensional analysis of observed structures using multipoint magnetic field measurements: Application to Cluster. *Geophysical Research Letters*, *32*, l12105. https://doi.org/10.1029/2005GL022454

Sonnerup, B. U. O. (1979). Magnetic field reconnection. *Solar System Plasma Physics*, *1*, 45–108.

Sonnerup, B. Ö., & Cahill, JrL. (1967). Magnetopause structure and attitude from Explorer 12 observations. *Journal of Geophysical Research*, *72*(1), 171–183.

Toledo-Redondo, S., André, M., Khotyaintsev, Y. V., Vaivads, A., Walsh, A., Li, W., et al. (2016). Cold ion demagnetization near the X-line of magnetic reconnection. *Geophysical Research Letters*, *43*, 6759–6767. https://doi.org/10.1002/2016GL069877

Toledo-Redondo, S., Dargent, J., Aunai, N., Lavraud, B., André, M., Li, W., et al. (2018). Perpendicular current reduction caused by cold ions of ionospheric origin in magnetic reconnection at the magnetopause: Particle-in-cell simulations and spacecraft observations. *Geophysical Research Letters*, *45*. https://doi.org/10.1029/2018GL079051

Toledo-Redondo, S., Vaivads, A., André, M., & Khotyaintsev, Y. V. (2015). Modification of the Hall physics in magnetic reconnection due to cold ions at the Earth's magnetopause. *Geophysical Research Letters*, *42*, 6146–6154. https://doi.org/10.1002/2015GL065129

Torbert, R., Russell, C., Magnes, W., Ergun, R., Lindqvist, P.-A., LeContel, O., et al. (2016). The fields instrument suite on MMS: scientific objectives, measurements, and data products. *Space Science Reviews*, *199*(1–4), 105–135.

Torkar, K., Nakamura, R., Tajmar, M., Scharlemann, C., Jeszenszky, H., Laky, G., et al. (2016). Active spacecraft potential control investigation. *Space Science Reviews*, *199*(1), 515–544. https://doi.org/10.1007/s11214-014-0049-3